Japanese Journal of Applied Physics

The Japan Society of Applied Physics

REGULAR PAPERS

Niobium doping induced morphological changes and enhanced photocatalytic performance of anatase TiO_2

To cite this article: Ming-Chung Wu *et al* 2017 *Jpn. J. Appl. Phys.* **56** 04CP07

View the article online for updates and enhancements.

Related content

- Bismuth doping effect on crystal structure and photodegradation activity of Bi–TiO_2 nanoparticles
Ming-Chung Wu, Yin-Hsuan Chang and Ting-Han Lin
- Mechanism of strong visible light photocatalysis by Ag2O-nanoparticle-decorated monoclinic TiO2(B) porous nanorods
Kamal Kumar Paul, Ramesh Ghosh and P K Giri
- Microwave-assisted synthesis of Mo-doped $H_{1-x}Sr_2Nb_{3-x}Mo_xO_{10}$ (x = 0, 0.05, 0.1, 0.15 and 0.2) with high photocatalytic activity
Xu Jing, Wei Yuelin, Huang Yunfang et al.

Recent citations

- Photocatalytic Performance of Cu-doped TiO 2 Nanofibers Treated by the Hydrothermal Synthesis and Air-thermal Treatment
Ming-Chung Wu *et al*

This content was downloaded from IP address 59.125.186.121 on 25/04/2019 at 06:28

Japanese Journal of Applied Physics **56**, 04CP07 (2017)
https://doi.org/10.7567/JJAP.56.04CP07

REGULAR PAPER

Niobium doping induced morphological changes and enhanced photocatalytic performance of anatase TiO_2

Ming-Chung Wu[1,2,3*], Ting-Han Lin[1], Jyun-Sian Chih[1], Kai-Chi Hsiao[1], and Po-Yeh Wu[1]

[1]*Department of Chemical and Materials Engineering, College of Engineering, Chang Gung University, Taoyuan 33302, Taiwan*
[2]*Center for Reliability Sciences & Technologies, Chang Gung University, Taoyuan 33302, Taiwan*
[3]*Division of Neonatology, Department of Pediatrics, Chang Gung Memorial Hospital, Taoyuan 33305, Taiwan*

*E-mail: mingchungwu@mail.cgu.edu.tw

Received October 11, 2016; revised December 27, 2016; accepted January 7, 2017; published online March 13, 2017

In order to develop high-performance photocatalysts that are easy to produce even in industrial quantities, we developed a facile method of preparing niobium-doped titanium dioxide (Nb:TiO_2) by hydrothermal synthesis and followed by thermal annealing treatment. Niobium-ion doping has been considered as an effective way to improve Nb:TiO_2 performance for applications in photocatalysis. Niobium-ion doping of anatase TiO_2 induced the morphological changes of Nb:TiO_2. Morphological analysis shows sub-microscale fibers at doping concentration lower than 1.00 mol % and nanoscale rods at the doping concentration higher than 1.00 mol %. For the catalyzed photodegradation of methyl orange under visible light irradiation, 0.50 mol % Nb:TiO_2 shows the highest activity among the synthesized Nb:TiO_2 specimens. Also, for photocatalytic hydrogen generation, its photocatalytic activity is even higher than that of commercial TiO_2-P25. In this study, we demonstrated the fabrication of a series of superior Nb:TiO_2 specimens. It is a reasonable alternative to commercial TiO_2 materials for various applications in the decomposition of organic dyes under visible light irradiation. © 2017 The Japan Society of Applied Physics

1. Introduction

Anatase TiO_2 is one of the most important materials, because it exhibits the high performance applications in photocatalysis, solar cells, and transparent conducting oxide films.[1–7] It has been found to be very active in the treatment of wastewaters containing a broad range of organic pollutants that are used in industries and daily life.[8–12] In particular, anatase TiO_2 is often cited as the best choice for green energy materials owing to its many advantages, such as thermal and chemical stability, inexpensiveness, ease of production and use, and being human- and environment-friendly.[13–15] However, anatase TiO_2 is not sufficiently suitable for realistic applications owing to its large bandgap, since it only utilizes the ultraviolet range of solar radiation.[16–19] Ultraviolet light has only 5% of solar energy. A question arises on how to convert solar energy to abundant electricity, which has become an important issue in the scientific field.

Much effort has been made to enhance the absorbing capability of TiO_2 over the visible spectrum by doping it with metal.[14,20,21] The photocatalytic activity of metal-doped TiO_2 substantially depends on the characteristics of the dopant, the concentration of dopant ions, the method of preparation, and the thermal and reductive treatment of TiO_2.[14,22–27] Niobium-doped TiO_2 (Nb:TiO_2) has attracted much interest owing to its high photocatalytic activity in the degradation of pollutants and dyes. The ionic radius of Nb^{5+} (~0.64 Å) is only slightly larger than that of Ti^{4+} (~0.61 Å),[28] which suggests that Nb^{5+} can easily be doped into the TiO_2 lattice. As a result, Nb doping will introduce donor levels below the conduction band of TiO_2. Nb:TiO_2 could thus enhance visible light absorption with a redshift of the optical absorption edge. Znad et al. prepared various Nb:TiO_2 materials by a simple impregnation method, namely, a Nb dopant is introduced to inhibit the TiO_2 phase transformation from anatase to rutile and to hinder grain growth during thermal treatment.[29] Yang et al. adopted an ultrasonic spray pyrolysis method to prepare Nb:TiO_2 porous microspheres for photocatalytic applications. The grain size of Nb:TiO_2 porous microspheres is decreased by increasing the doping concentration, which affects the surface area of microspheres, pore size distribution, and the absorption spectra shift from the ultraviolet band to the visible band.[30] The phase transition behavior and doping concentration in pressure-treated Nb:TiO_2 were systematically investigated by in situ synchrotron X-ray diffraction and Raman spectroscopy. The obtained structural information provides direct evidence for the packing correlation with electron transport in semiconductors.[31] The photocatalytic activity of metal-doped TiO_2 photocatalysts substantially depends on the characteristics of the dopant, the concentration of dopant ions, the method of preparation, and the thermal and reductive treatments.[14,22–27] The extended light absorption and the suppression of electron–hole pair recombination can enhance photocatalytic activity.[31,32] Despite the large UV–vis absorption and the strong surface interaction, Mattsson et al. reported that the decomposition rate is still low in Nb:TiO_2 films.[32] The low photocatalytic activity could be attributed to the increased electron–hole recombination rate owing to the Nb=O cluster and the formation of vacancy sites in the anatase lattice.

In this study, we elucidated the niobium doping effects on anatase TiO_2 in terms of morphological change and photocatalytic activity. A series of fiber-shaped and/or rod-shaped Nb:TiO_2 specimens were developed using well-defined doping concentrations. The optimal Nb doping concentrations were studied to find the high photocatalytic activity. The photodecolorization of an organic dye for various Nb:TiO_2 specimens under UV and visible light irradiations was measured and examined in detail. Hopefully, the developed Nb:TiO_2 will be one of the commercial photocatalyst candidates for applications in the decomposition of organic dyes under visible light irradiation.

2. Experimental procedure

Various Nb:TiO_2 specimens were prepared by suspending 1.00 g of TiO_2 anatase powder (Acros Organics, 98%) and various amounts of niobium chloride ($NbCl_5$; Acros Organics, 99.999%) in 25 mL of 10.0 M NaOH aqueous solution, followed by treatment in a teflon-lined autoclave at 150 °C for 24 h. The product was washed with deionized

 © 2017 The Japan Society of Applied Physics

water, then filtered and dried in air at 70 °C. Then, it was washed with 0.10 M HCl to exchange sodium ions for protons. The procedure was repeated twice. Finally, various hydrogen sodium titanate specimens doped with different Nb ion concentrations were prepared successfully. These products were calcined at 600 °C at a heating rate of 5 °C/min for 12 h, as in our previous study.[33] Hydrogen sodium titanate calcined at 600 °C only consists of the anatase TiO_2 phase, and it shows high photocatalytic activity. For Pd-decorated Nb:TiO_2, 29.2 mg of palladium(II) acetylacetonate (Aldrich, 99%) was dissolved in 200 mL of acetone first and mixed with 1.0 g of Nb:TiO_2 by ultrasonic agitation for 3 h. The resultant mixture was stirred for 6 h. After evaporating the solvent at 80 °C in N_2 atmosphere, the samples were calcined in air at 300 °C for 2 h, and then reduced at 300 °C in 15% H_2 (in N_2 buffer) flow for 4 h. Pd-decorated Nb:TiO_2 loaded with 1.0 wt % metal was thus prepared.

For Raman scattering measurement, these specimens were positioned on a high-resolution piezoelectric stage of a scanning microscope (WiTec Alpha300S) and excited by a 632.8 nm He–Ne laser (25 mW). The laser beam was focused with a 100× objective lens (Nikon plane objective, NA ~ 0.9). The diameter of the laser beam was focused at about 10 μm. A synchrotron X-ray diffractometer (National Synchrotron Radiation Research Center, 13A1/SW60-X-ray scattering) was used to measure the crystalline structure. Transmission electron microscopy (TEM; JEOL JEM-ARM200FTH) was used to observe Nb:TiO_2 microstructures. The extinction spectra of Nb:TiO_2 were collected using an absorption spectrophotometer (JASCO V-630) at 300–900 nm. X-ray photoelectron spectrometry (XPS; ULVAC-PHI) was used to examine the Nb:TiO_2 specimens by Al Kα radiation at a photoelectron take-off angle of 45° in high vacuum (~10^{-7} Torr).

Photocatalytic hydrogen generation tests were carried out in a 1 : 1 volume ratio mixture of ethanol and water (total, 2.0 L), in which 10.0 mg of Nb:TiO_2 was suspended. The mixture was stirred at room temperature. As the light source, six lamps were placed in a hexagonal arrangement around the reactor. The light source includes UV-B lamps (Sankyo Denki G8T5E UV-B; wavelength at maximum emission, 312 nm; power, 8.0 W) and visible lamps (Goodly F8T5/D; power, 8.0 W). For UV light and visible light irradiations, the light intensity is ~1.12 mW/cm^2, and the total irradiation area is about 600 cm^2. To prevent the sedimentation of the catalyst powders, nitrogen (99.999%) was bubbled through the reactor at a flow rate of 400 mL/min as the purging gas for evolving gaseous products. The outlet gas of the reactor was connected to a cold trap, a molecular sieve, and a hydrogen analyzer (Status Scientific Controls FGD3).

The Nb:TiO_2 specimens with various doping concentrations were tested in terms of degradation of methyl orange, which is a commonly used model reaction in photocatalysis. 20.0 mg of the catalyst was sonicated for 2 min in 150 mL of 10.0 mg/L methyl orange (Acros Organics, pure) aqueous solution. Before the actual photodegradation experiments, the suspensions were left to relax for 10 min in order to minimize the error of dye concentration measurements caused by the initial surface adsorption. As light sources, six lamps were placed in a hexagonal arrangement around the reactor. The suspension solution was irradiated with different light sources with vigorous stirring under ambient conditions. The light sources included UV-B lamps and visible lamps. For UV and visible light irradiations, the light intensity was ~0.39 mW/cm^2, and the total irradiation area was about 150 cm^2. After centrifugation for 15 min at 5000 rpm, the absorption spectra of the retained methyl orange and its derivatives in the supernatant were recorded using an absorption spectrophotometer (JASCO V-630) at 300–900 nm. The concentration of methyl orange was calculated from the absorbance at $\lambda = 464$ nm and extrapolated by a previously plotted calibration curve.

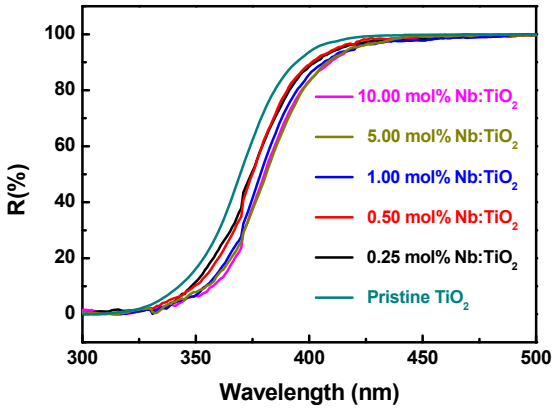

Fig. 1. (Color online) Reflection spectra of pristine TiO_2 and Nb:TiO_2 doped with various Nb concentrations and calcined at 600 °C for 12 h.

3. Results and discussion

In order to determine the correlation between Nb doping concentration and optical characteristics, the normalized reflectance spectra of pristine TiO_2 NFs and Nb:TiO_2 with various doping concentrations were measured using a UV–visible spectrophotometer. From the reflectance spectra shown in Fig. 1, we observe that the reflectance spectra exhibited a redshift when niobium ion was doped into Nb:TiO_2. The bandgaps of pristine TiO_2 NFs and 0.25, 0.50, 1.00, 5.00, and 10.00 mol % Nb:TiO_2 specimens were calculated from the UV–vis reflectance spectra and their values were 3.75, 3.62, 3.60, 3.52, 3.51, and 3.51 eV, respectively. These results suggest that the bandgap of Nb:TiO_2 decreased from 3.75 eV with respect to niobium ion doping concentration.

A Raman spectrometer was used to obtain information about the vibrational modes of Nb:TiO_2. We aim to observe the phase transformation of various Nb:TiO_2 specimens with increasing Nb doping concentration, as shown in Fig. 2. Pristine TiO_2 NFs displays Raman bands at 144, 200, 398, 515, 517, and 640 cm^{-1} with the Raman bands at 515 and 517 cm^{-1} superimposed. These bands can be attributed to the six Raman-active modes of the anatase phase with the symmetries of E_g, E_g, B_{1g}, A_{1g}, B_{1g}, and E_g, respectively.[34] Obviously, all of the Nb:TiO_2 specimens are mostly in the anatase phase, even when the Nb doping concentration is as high as 10.00 mol %.

The crystal structure of pristine TiO_2 and various Nb:TiO_2 specimens were further characterized using a synchrotron X-ray diffractometer ($\lambda \sim 1.025$ Å). The acquired synchrotron X-ray spectra are shown in Fig. 3(a). The main crystal structure of the anatase phase of the various Nb:TiO_2

© 2017 The Japan Society of Applied Physics

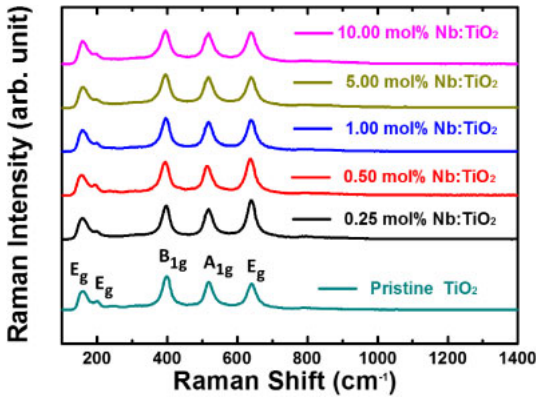

Fig. 2. (Color online) Raman spectra of pristine TiO_2 and various Nb:TiO_2 specimens doped at different Nb concentrations and calcined at 600 °C for 12 h.

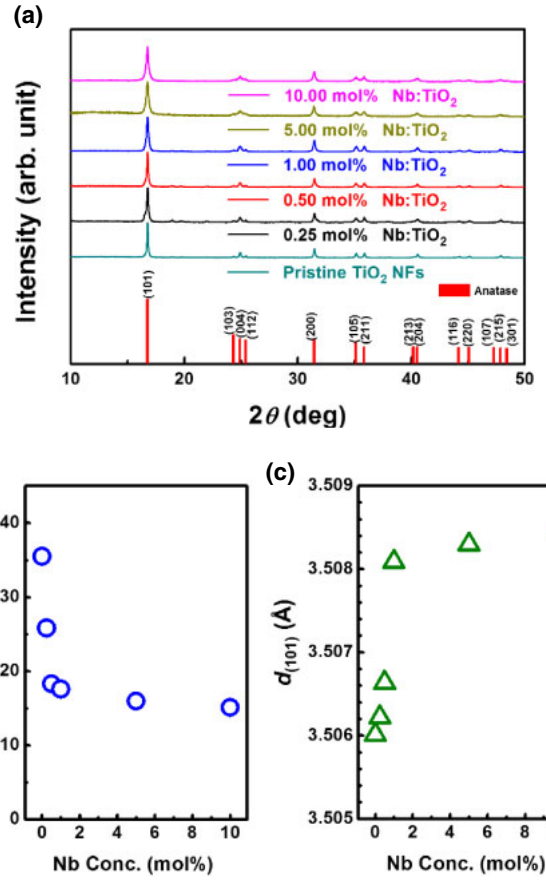

Fig. 3. (Color online) (a) Synchrotron X-ray spectra of pristine TiO_2 and various Nb:TiO_2 specimens calcined at 600 °C for 12 h, (b) estimated crystallite size and (c) d spacing of (101) plane of pristine TiO_2 and various Nb:TiO_2 specimens.

specimens is confirmed. The signals of synchrotron X-ray spectra indicate a body-centered tetragonal lattice structure (JCPDS No. 89-4921) of anatase TiO_2, with the lattice constants $a = b = 3.78$ Å and $c = 9.51$ Å. The nanocrystallite size is calculated using Scherrer's equation as shown in Fig. 3(b).[35] The crystallite size decreases from 35.5 to 15.1 nm in accordance with 1.00 mol % niobium doping concentration. The obtained synchrotron X-ray spectra show that the peak shift of the anatase TiO_2(101) plane occurs toward smaller angles with increasing Nb concentration. The

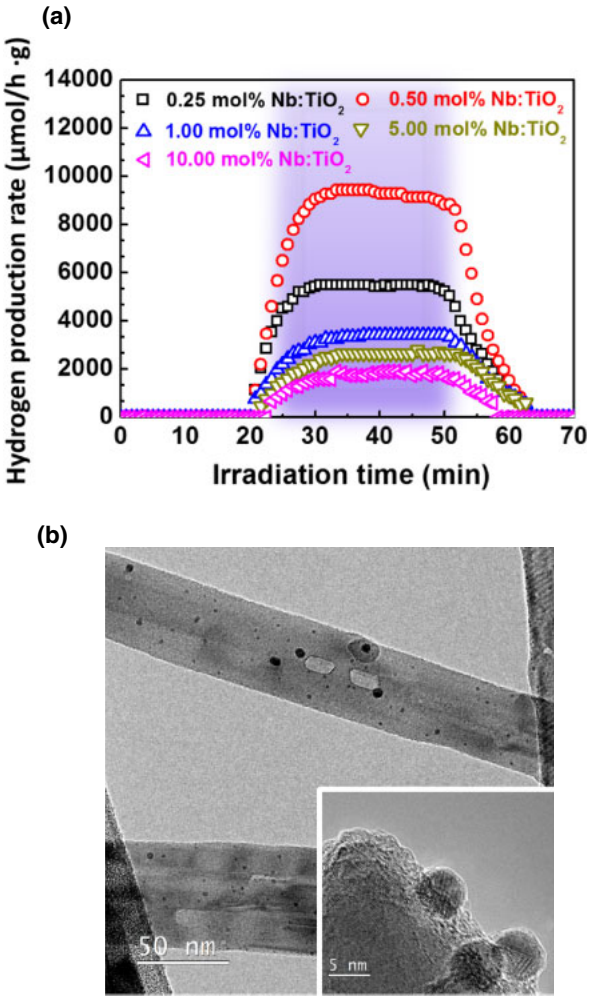

Fig. 4. (Color online) (a) Photocatalytic hydrogen production rates of various Pd-decorated Nb:TiO_2 specimens reduced at 300 °C for 4 h under UV irradiation. (b) TEM images of Pd–0.50 mol % Nb:TiO_2.

d spacing of the (101) plane increases with the increase in Nb doping concentration owing to the radius of a Nb^{5+} ion being relatively larger than that of a Ti^{4+} ion, as shown in Fig. 3(c).[36]

For applications, all the synthesized Nb:TiO_2 specimens without metal nanoparticle decoration show undetectable hydrogen production under UV irradiation. Thus, we decorated 1.0 wt % Pd nanoparticles on the Nb:TiO_2 surface to increase hydrogen production efficiency, as shown in Fig. 4(a). When the Nb doping concentration exceeds 0.50 mol %, the photocatalytic hydrogen production rate of Nb:TiO_2 under UV irradiation decreases significantly, which could be due to the large amount of Nb doped. It inhibited the electron and/or hole transport in Nb:TiO_2. Pd–0.50 mol % Nb:TiO_2 shows the highest rate of photocatalytic hydrogen production, which reaches ~9,400 μmol·g^{-1}·h^{-1} under UV irradiation. However, various Nb:TiO_2 specimens decorated with Pd nanoparticles under visible light irradiation show no detectable hydrogen production. This could be due to the visible light energy being insufficient to excite the TiO_2 materials to produce electron/hole pairs. The microstructure of Pd–0.50 mol % Nb:TiO_2 was also observed by transmission electron microscopy. The length of Pd–0.50 mol % Nb:TiO_2 was up to 5–10 μm and its diameter ranged from 80 to 150 nm. Pd-based nanoparticles distributed on the surface

© 2017 The Japan Society of Applied Physics

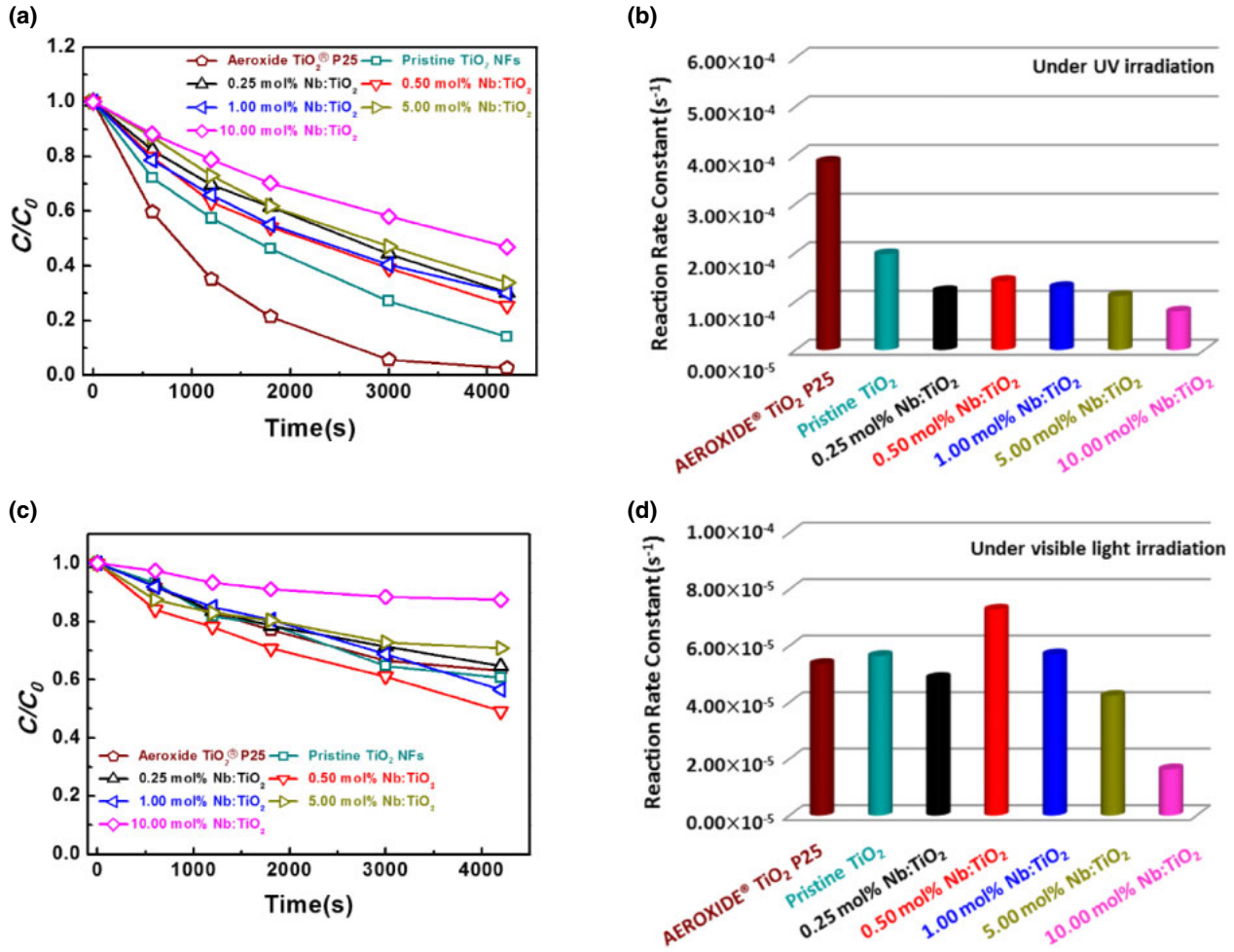

Fig. 5. (Color online) (a, c) Plots of C/C_0 and (b, d) column charts of pristine TiO_2 NFs and Nb:TiO_2 doped at various concentrations and calcined at 600 °C for 12 h in relation to the photodegradation of methyl orange under certain light source irradiations: (a, b) UV light and (c, d) visible light.

of 0.50 mol % Nb:TiO_2 present a uniform size distribution with an average particle diameter of 5.5 nm, as shown in the inset of Fig. 4(b).

In order to understand the correlation between photodegradation activity and Nb doping concentration for Nb:TiO_2, we measured the photodegradation activities of various Nb:TiO_2 specimens under irradiation from different light sources. The absorption spectra of methyl orange as a function of time under irradiation from different light sources were recorded. The absorbance measured at $\lambda = 464$ nm was used to calculate methyl orange concentration using a calibration curve measured previously. The color of the suspension changed from the initial cloudy color to colorless. The C/C_0 curve, in which C is the concentration of the dye at time t and C_0 is the initial concentration, for the photodegradation of methyl orange at different times using various Nb:TiO_2 specimens is obtained. The TiO_2-catalyzed photodegradation of organic dyes usually follows the Langmuir–Hinshelwood kinetics, which can be simplified to an apparent first-order kinetics at lower initial dye concentrations, mathematically described as $\ln(C_0/C) = kt$, where k is the apparent reaction rate constant.[20,37] For the photodegradation activity of these Nb:TiO_2 specimens under UV irradiation, 0.50 mol % Nb:TiO_2 shows the highest photodegradation reaction rate constant [Figs. 5(a) and 5(b)]. Moreover, all the Nb:TiO_2 specimens were tested under visible light irradiation. As shown in Figs. 5(c) and 5(d), 0.50 mol % Nb:TiO_2 also shows the highest activity under visible light irradiation among all the TiO_2-based materials. The photodegradation reaction rate constants under UV and visible light irradiations are shown using bar charts in Figs. 5(b) and 5(d), respectively. 0.50 mol % Nb:TiO_2 shows the highest activity of the photodegradation of methyl orange under UV and visible light irradiations owing to the optimal parameters for the photon absorption behavior, chemical composition, crystal structure, and active surface area. The optimal Nb doping concentration could enhance ethanol oxidation and photoinduced hydrogen evolution, resulting in an increased photocatalytic activity.

The actual Nb ion concentration in Nb:TiO_2 is important information to understand the Nb doping effect on TiO_2 materials. The Nb ion concentrations in Nb:TiO_2 were investigated by XPS, as shown in Table I. For pristine TiO_2, there is no Nb signal observed in the XPS spectrum. For various Nb:TiO_2 specimens, the plots exhibited peaks at 207.6 and 210.4 eV assigned to the $3d_{5/2}$ and $3d_{3/2}$ states of Nb, respectively.[37,38] It is interesting to note that 5.00 mol % for Nb:TiO_2 and 10.00 mol % for Nb:TiO_2 measured by XPS are less than the theoretical values. This could be due to the fact that the synthesized Nb:TiO_2 must be washed with deionized water before its calcination. The morphologies of pristine TiO_2 and various Nb:TiO_2 specimens are shown in

© 2017 The Japan Society of Applied Physics

Table I. Theoretical and experimental niobium concentrations in pristine TiO_2 and various Nb:TiO_2 samples calcined at 600 °C for 12 h.

Material	Nb concentration (mol %)	
	Theoretical value	XPS analysis
Pristine TiO_2	0.00	0.00
0.25 mol % Nb:TiO_2	0.25	0.26
0.50 mol % Nb:TiO_2	0.50	0.35
1.00 mol % Nb:TiO_2	1.00	1.08
5.00 mol % Nb:TiO_2	5.00	3.18
10.00 mol % Nb:TiO_2	10.00	4.69

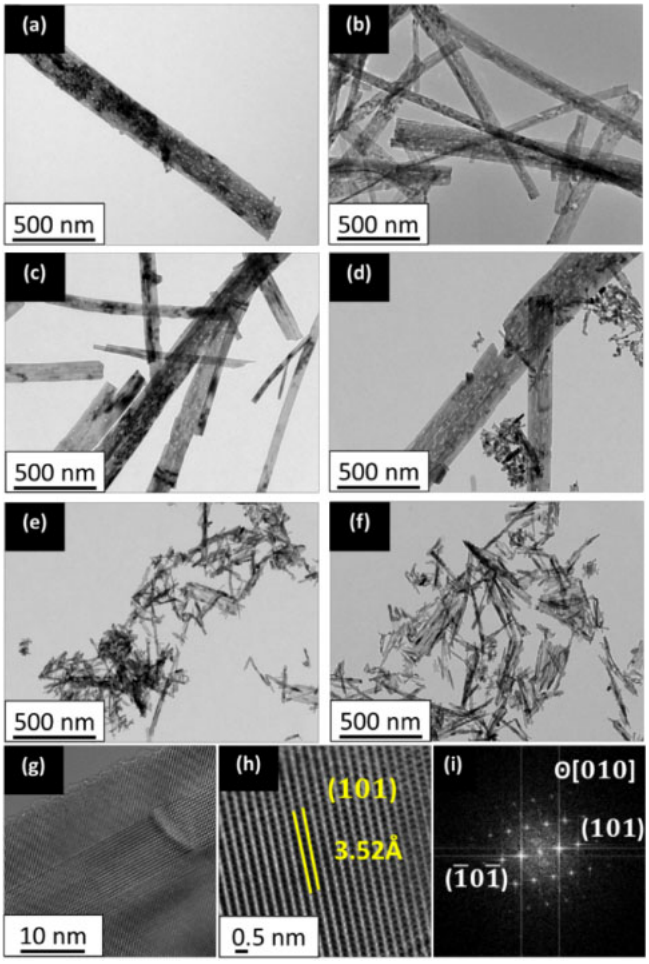

Fig. 6. (Color online) TEM images of (a) pristine TiO_2, (b) 0.25 mol %, (c) 0.50 mol %, (d) 1.00 mol %, (e) 5.00 mol %, and (f) 10.00 mol % Nb:TiO_2 calcined at 600 °C for 12 h. (g) High-resolution TEM image, (h) high-magnification lattice image, and (i) corresponding fast-Fourier-transformed pattern of 0.50 mol % Nb:TiO_2.

Fig. 6. We observe that Nb doping results in the morphological changes of Nb:TiO_2. The as-made pristine TiO_2 material has a length of up to 5–10 μm and a diameter of ~100–200 nm [Fig. 6(a)]. The morphologies of the 0.25 mol % Nb:TiO_2 and 0.50 mol % Nb:TiO_2 are similar to that of the pristine TiO_2, as shown in Figs. 6(b) and 6(c). On the other hand, some small rod-shaped materials are observed, when the doping concentration reaches 1.00 mol % [Fig. 6(d)]. The diameter of Nb:TiO_2 decreases to ~50 nm when the doping concentration is over 5.00 mol %, as shown in Figs. 6(e) and 6(f), because Nb:TiO_2 broke into small pieces and became rod-shaped. When the Nb doping concentration is over 5.00 mol %, the Nb doping results in the incorporation of a substantial number of Nb ions into the TiO_2 lattice. The morphological scale of synthesized Nb:TiO_2 catalysts decreases with Nb doping concentration. Figure 6(g) shows a high-resolution TEM image of 0.50 mol % Nb:TiO_2. The high-magnification lattice images with the corresponding fast-Fourier-transformed pattern of this specimen are shown in Figs. 6(h) and 6(i). An increased d spacing of the (101) crystal plane is observed for 0.50 mol % Nb:TiO_2. The minor change in (101) spacing is from 3.46 Å in pristine TiO_2 to 3.52 Å in 0.50 mol % Nb:TiO_2. The results indicate that Nb doping causes the incorporation of a substantial number of Nb ions into the TiO_2 lattice. The morphological scale of as-made Nb:TiO_2 diminished with increasing Nb doping concentration. The fragmentation of the microstructure of Nb:TiO_2 was the result of doping Nb ions into TiO_2. Multimorphological Nb:TiO_2 materials, including the sub-microscale fiber materials (0.25, 0.50, and 1.00 mol % Nb:TiO_2) and the nanoscale rod materials (5.00 and 10.00 mol % Nb:TiO_2), were synthesized successfully.

4. Conclusions

The synthesized Nb:TiO_2 specimens doped at different Nb ion doping concentration showed different morphologies, including sub-microscale fibers (<1.00 mol % Nb doping) and nanoscale rods (>5.00 mol % Nb doping). Raman spectrum analysis and XRD results confirmed that the Nb:TiO_2 specimens were still mostly in the anatase phase and niobium doping did not significantly induce crystalline structural changes. The Nb:TiO_2 doped with 0.50 mol % Nb exhibited the highest activity of catalyzed photodegradation of methyl orange under UV or visible light irradiation. The obtained Nb:TiO_2 may be a reasonable alternative to commercial photocatalysts for photocatalytic applications in the decomposition of organic dyes.

Acknowledgements

The authors thank Professor Wei-Fang Su of National Taiwan University and the Dr. Ming-Tao Lee group (BL-13A1) of the National Synchrotron Radiation Research Center for useful discussion and suggestions. The authors also thank the staff of the Instrumentation Center of National Tsing Hua University for HRTEM analysis. The authors acknowledge the financial support of the Ministry of Science and Technology, Taiwan (MOST 105-2221-E-182-011, MOST 105-2632-E-182-001, and MOST 105-3113-E-002-010) and Chang Gung Memorial Hospital, Taiwan (CMRPD2E0071, CMRPD2F0161, and BMRPC74).

1) K. Hashimoto, H. Irie, and A. Fujishima, Jpn. J. Appl. Phys. **44**, 8269 (2005).
2) I. S. Cho, Z. Chen, A. J. Forman, D. R. Kim, P. M. Rao, T. F. Jaramillo, and X. Zheng, Nano Lett. **11**, 4978 (2011).
3) A. Fujishima and K. Honda, Nature **238**, 37 (1972).
4) M. Fujihira, Y. Satoh, and T. Osa, Nature **293**, 206 (1981).
5) A. J. Nozik, Nature **257**, 383 (1975).
6) S. Kajita, T. Yoshida, N. Ohno, T. Ishida, and D. Kitaoka, Jpn. J. Appl. Phys. **55**, 106202 (2016).
7) C. Shimada, K. Kitamura, and S. Shiratori, Jpn. J. Appl. Phys. **51**, 044106 (2012).
8) M. Ozawa, H. Matui, and S. Suzuki, Jpn. J. Appl. Phys. **55**, 01AG04

© 2017 The Japan Society of Applied Physics

(2016).
9) T. Ochiai, T. Hoshi, H. Slimen, K. Nakata, T. Murakami, H. Tatejima, Y. Koide, A. Houas, T. Horie, Y. Morito, and A. Fujishima, Catal. Sci. Technol. **1**, 1324 (2011).
10) D. M. Tobaldi, R. C. Pullar, A. S. Škapin, M. P. Seabra, and J. A. Labrincha, Mater. Res. Bull. **50**, 183 (2014).
11) X. Zhang, J. Yao, D. Li, X. Chen, H. Wang, L. Y. Yeo, and J. R. Friend, Mater. Res. Bull. **55**, 13 (2014).
12) W. Wu, X. Xue, X. Jiang, Y. Zhang, Y. Wu, and C. Pan, AIP Adv. **5**, 057105 (2015).
13) D. Rafieian, W. Ogieglo, T. Savenije, and R. G. H. Lammertink, AIP Adv. **5**, 097168 (2015).
14) M.-C. Wu, J. Hiltunen, A. Sápi, A. Avila, W. Larsson, H.-C. Liao, M. Huuhtanen, G. Tóth, A. Shchukarev, N. Laufer, Á. Kukovecz, Z. Kónya, J.-P. Mikkola, R. Keiski, W.-F. Su, Y.-F. Chen, H. Jantunen, P. M. Ajayan, R. Vajtai, and K. Kordás, ACS Nano **5**, 5025 (2011).
15) M.-C. Wu, H.-C. Liao, Y.-C. Cho, G. Toth, Y.-F. Chen, W.-F. Su, and K. Kordas, J. Mater. Chem. A **1**, 5715 (2013).
16) D. A. H. Hanaor and C. C. Sorrell, J. Mater. Sci. **46**, 855 (2011).
17) I. K. Konstantinou and T. A. Albanis, Appl. Catal. B **49**, 1 (2004).
18) P. Montes-Navajas, M. Serra, and H. Garcia, Catal. Sci. Technol. **3**, 2252 (2013).
19) M.-C. Wu, G. Tóth, A. Sápi, A.-R. Leino, Z. Kónya, Á. Kukovecz, W.-F. Su, and K. Kordás, J. Nanosci. Nanotechnol. **12**, 1421 (2012).
20) M.-C. Wu, J.-S. Chih, and W.-K. Huang, CrystEngComm **16**, 10692 (2014).
21) T. Nikolay, L. Larina, O. Shevaleevskiy, and B. T. Ahn, Energy Environ. Sci. **4**, 1480 (2011).
22) T. Huang, S. Mao, J. Yu, Z. Wen, G. Lu, and J. Chen, RSC Adv. **3**, 16657 (2013).
23) T. Liu and H. Zhang, RSC Adv. **3**, 16255 (2013).
24) D. P. Macwan, P. N. Dave, and S. Chaturvedi, J. Mater. Sci. **46**, 3669 (2011).
25) A. Pandikumar, K. Sivaranjani, C. S. Gopinath, and R. Ramaraj, RSC Adv. **3**, 13390 (2013).
26) G. Pótári, D. Madarász, L. Nagy, B. László, A. Sápi, A. Oszkó, A. Kukovecz, A. Erdőhelyi, Z. Kónya, and J. Kiss, Langmuir **29**, 3061 (2013).
27) M.-C. Wu, A. Sápi, A. Avila, M. Szabó, J. Hiltunen, M. Huuhtanen, G. Tóth, Á. Kukovecz, Z. Kónya, R. Keiski, W.-F. Su, H. Jantunen, and K. Kordás, Nano Res. **4**, 360 (2011).
28) Y. Kou, J. Yang, B. Li, and S. Fu, Mater. Res. Bull. **63**, 105 (2015).
29) H. Znad, M. H. Ang, and M. O. Tade, Int. J. Photoenergy **2012**, 1 (2012).
30) J. Yang, X. Zhang, C. Wang, P. Sun, L. Wang, B. Xia, and Y. Liu, Solid State Sci. **14**, 139 (2012).
31) X. Lü, W. Yang, Z. Quan, T. Lin, L. Bai, L. Wang, F. Huang, and Y. Zhao, J. Am. Chem. Soc. **136**, 419 (2014).
32) A. Mattsson, M. Leideborg, K. Larsson, G. Westin, and L. Österlund, J. Phys. Chem. B **110**, 1210 (2006).
33) M.-C. Wu, G. Toth, A. Sapi, A. R. Leino, Z. Konya, A. Kukovecz, W.-F. Su, and K. Kordas, J. Nanosci. Nanotechnol. **12**, 1421 (2012).
34) J. Zhang, M. Li, Z. Feng, J. Chen, and C. Li, J. Phys. Chem. B **110**, 927 (2006).
35) A. L. Patterson, Phys. Rev. **56**, 978 (1939).
36) H. Su, Y.-T. Huang, Y.-H. Chang, P. Zhai, N. Y. Hau, P. C. H. Cheung, W.-T. Yeh, T.-C. Wei, and S.-P. Feng, Electrochim. Acta **182**, 230 (2015).
37) M. Z. Atashbar, H. T. Sun, B. Gong, W. Wlodarski, and R. Lamb, Thin Solid Films **326**, 238 (1998).
38) A. Sasahara and M. Tomitori, J. Phys. Chem. C **117**, 17680 (2013).

© 2017 The Japan Society of Applied Physics